

Decoupling of the $S = 1/2$ antiferromagnetic zig-zag ladder with anisotropy

V. R. Vieira

Departamento de Física and CFIF, Instituto Superior Técnico, Av. Rovisco Pais, 1049-001 Lisboa, Portugal

N. Guihéry

*Laboratoire de Physique Quantique, Université Paul Sabatier, F-31062 Toulouse, France and
CFIF, Instituto Superior Técnico, Av. Rovisco Pais, 1049-001 Lisboa, Portugal*

J. P. Rodriguez

Department of Physics and Astronomy, California State University, Los Angeles, California 90032, USA

P. D. Sacramento

*Departamento de Física and CFIF, Instituto Superior Técnico, Av. Rovisco Pais, 1049-001 Lisboa, Portugal
(November 3, 2018)*

The spin-1/2 antiferromagnetic zig-zag ladder is studied by exact diagonalization of small systems in the regime of weak inter-chain coupling. A gapless phase with quasi long-range spiral correlations has been predicted to occur in this regime if easy-plane (XY) anisotropy is present. We find in general that the finite zig-zag ladder shows three phases: a gapless collinear phase, a dimer phase and a spiral phase. We study the level crossings of the spectrum, the dimer correlation function, the structure factor and the spin stiffness within these phases, as well as at the transition points. As the inter-chain coupling decreases we observe a transition in the anisotropic XY case from a phase with a gap to a gapless phase that is best described by two decoupled antiferromagnetic chains. The isotropic and the anisotropic XY cases are found to be qualitatively the same, however, in the regime of weak inter-chain coupling for the small systems studied here. We attribute this to a finite-size effect in the isotropic zig-zag case that results from exponentially diverging antiferromagnetic correlations in the weak-coupling limit.

PACS numbers:

I. INTRODUCTION

Antiferromagnetic ladder systems have attracted much interest recently.¹ On the theoretical side they interpolate between the well studied antiferromagnetic chain² and two dimensional antiferromagnets.³ The evolution between 1D and 2D spin-1/2 antiferromagnetism is not necessarily smooth, however. In particular, the n -leg ladder shows a remarkable alternating property in the spectrum as the number of legs is even or odd.⁴ The spectrum has a gap for an even number of legs while it is gapless for an odd number of legs. This is similar to the difference between integer (spin-gap) and half-odd-integer (gapless) spin chains⁵. In the limit of strong-coupling between the two chains the two-leg ladder is essentially composed of weakly interacting singlets that form across the rungs. The lowest excitation is the promotion of a rung singlet to a triplet with an excitation energy of the order of the inter-chain coupling. This spin gap remains nonvanishing even for small inter-chain coupling due to the fact that a single antiferromagnetic chain is critical.⁶ In the case of purely Ising coupled chains the gap appears for all values of n .⁷

The antiferromagnetic zigzag ladder has also attracted interest recently, particularly in the context of experimental systems with low-dimensional magnetic struc-

tures like that of Cs_2CuCl_4 ⁸. It is also interesting from a theoretical point of view because it is a frustrated system (see Fig. 1). Indeed, the zig-zag ladder is equivalent to a single antiferromagnetic chain with next-nearest-neighbor interactions. In this paper we consider the spin-1/2 antiferromagnetic zigzag ladder with anisotropy. The isotropic case has been studied before⁹⁻¹⁴ as a function of the coupling parameter, $j = J_2/J_1$, which is the ratio of the next-nearest-neighbor interaction, J_2 , to the nearest-neighbor interaction, J_1 . As j increases, the system goes from gapless (single chain) to a dimer phase and then to a spiral phase, where the structure factor has a maximum at a momentum $\pi/2 < q < \pi$. The system has a spin gap in these last two phases, and it therefore only displays short-range order. In the limit that the intra-chain interaction is much larger than the inter-chain interaction ($j \rightarrow \infty$) the two chains decouple and a gapless single chain behavior is recovered. It has been argued that this only happens, strictly speaking, at $j = \infty$: the spin gap becomes exponentially small as j grows, but it remains non-vanishing.¹³ Recently, on the other hand, it has been proposed that incommensurate quasi-long-range spin correlations should be observed if easy-plane (XY) anisotropy is included in the zigzag ladder.¹⁵ This is argued to be due to the presence of a “twist” term that results from the inter-chain interaction. It has been

proposed that there is one gapless mode and one mode with a gap in the regime of strong XY anisotropy in the inter-chain coupling. Another prediction of this work is the existence of spontaneous local spin currents. This, however, has been refuted in ref. 16. Also, other recent numerical work¹⁷ has failed to confirm the gapless nature of the groundstate in the anisotropic XY case at weak interchain coupling. Recent Density Matrix Renormalization Group (DMRG) results¹⁸ suggest, however, that the zig-zag ladder does indeed show a gapless chiral phase as predicted in ref. 15.

In this paper we use exact diagonalizations, the modified Lanczos method¹⁹ and the Davidson method²⁰ to address the possibility of a transition from a spin-gap regime to a gapless regime as a function of j when anisotropy is present in small $S = 1/2$ antiferromagnetic zig-zag ladders. We compute various probes to identify the different phases and study their behavior close to the transition points. We study in particular the spin stiffness, the dimer correlation function, the structure factor, and analyze in detail the spectrum in the various parameter regimes. Since the zig-zag ladder effectively has both nearest-neighbor and second neighbor interactions, a stiffness tensor is required to account for these two types of interactions. The eigenvalues of this 2×2 matrix then become the natural spin rigidities that we use to clarify the behavior of the system in the various regimes. The stiffness of a system is a particularly good measure of the long-range nature of the groundstate. Introducing twisted boundary conditions leads to a response in the energy if the quantum states are extended (gapless case). On the other hand, the energy is insensitive to a change in the boundary conditions if the quantum states are localized (spin-gap case). Therefore, the stiffness with respect to such a twist is positive if the system is gapless and it is zero if the system has a gap. Also, the dimer correlation function naturally signals the dimer phase while the structure factor is a natural way to detect and study the spiral phase.

Our results are consistent with a gapless excitation spectrum in the case of XY anisotropy at weak inter-chain coupling. We obtain qualitatively similar results for the isotropic case, however. This is most likely a finite size effect due to the exponentially small spin gap that persists in the isotropic zig-zag at weak coupling in the thermodynamic limit.¹³ In fact, we show that the phase diagram that is obtained from the analysis of the spectrum for finite systems may be consistent with the field theory prediction¹⁵ after performing extrapolations to the thermodynamic limit.

The paper is organized as follows: In section II we present the model and the quantities to be calculated. In section III we present our results and in section IV we summarize the work. Technical details concerning exact diagonalization are given in the Appendix. We also briefly review the extrapolation technique to the thermodynamic limit here.

II. MODEL AND PROBES

The anisotropic zigzag ladder is defined by the Hamiltonian

$$H = \frac{1}{2} J_1^{XY} \sum_i (S_i^+ S_{i+1}^- + S_i^- S_{i+1}^+) + J_1^z \sum_i S_i^z S_{i+1}^z + \frac{1}{2} J_2^{XY} \sum_i (S_i^+ S_{i+2}^- + S_i^- S_{i+2}^+) + J_2^z \sum_i S_i^z S_{i+2}^z. \quad (1)$$

The spin operators refer to spin $S = 1/2$ states, while the summation $i = 1, \dots, N$ runs along the “rib” of the zig-zag ladder. We shall parameterize the interactions by the coupling parameter $j = J_2^{XY}/J_1^{XY}$ and by the anisotropy parameter $J_1^z/J_1^{XY} = \Delta = J_2^z/J_2^{XY}$. (The isotropic case reduces to $j = J_2/J_1$ and $\Delta = 1$.) We will set $J_1^{XY} = 1$ henceforth. Consider first the nearest-neighbor Heisenberg chain with anisotropy, which corresponds to both the weak-coupling ($J_1 = 0$) and to the strong-coupling ($J_2 = 0$) limits of the zig-zag ladder (see Fig. 1). The spectrum is gapless for the case of XY anisotropy, $|\Delta| \leq 1$, as shown by the Bethe ansatz.²¹ The excitation spectrum consists of spin-1/2 particles dubbed spinons. Since flipping one spin represents a spin-1 excitation, the spinons can only be created in pairs. Therefore the conventional spin 1 magnons are deconfined into spin-1/2 spinons that propagate incoherently. In the regime where $\Delta \leq -1$, the groundstate is ferromagnetic. When $-1 \leq \Delta \leq 1$ the leading spin configuration is the Néel state with the staggered magnetization lying within the XY plane. At $\Delta = 1$ the groundstate is again in a Néel state, but with a staggered magnetization that can point in any direction. Last, the spectrum shows a gap in the Ising regime at $\Delta > 1$. The groundstate, on the other hand, displays strict long-range Néel order, with the staggered magnetization directed along the z axis.

We shall begin our study of the antiferromagnetic zig-zag ladder by analyzing the classical limit of the isotropic Heisenberg case first: $J_1^{XY} = J_\perp = J_\perp^z$ and $J_2^{XY} = J_\parallel = J_\parallel^z$ as $S \rightarrow \infty$. A spiral state $S_i^+ = S e^{i\theta_i}$ yields an energy per site of $E(\theta) = S^2 J_\parallel \cos(2\theta) + S^2 J_\perp \cos\theta$. This magnetic energy is minimized at a pitch angle θ_0 that satisfies $\cos\theta_0 = -\frac{1}{4} J_\perp / J_\parallel$ for inter-chain exchange couplings that are below a critical value $J_\perp^c = 4J_\parallel$. A ferromagnetic state on each chain occurs, on the other hand, at strong coupling $J_\perp > J_\perp^c$, with a pitch angle of $\theta_0 = \pi$. The spins are thus arranged antiparallel in between chains. To summarize, the system is in a spiral phase for $J_\perp < 4J_\parallel$, while it is in a collinear phase for $J_\perp > 4J_\parallel$. The same holds true when only XY -coupling exists. In the case of Ising coupling only, on the other hand, we have the effective model $H = J_\parallel^z \sum_i S_i^z S_{i+2}^z + J_\perp^z \sum_i S_i^z S_{i+1}^z$. There are two possible groundstates. The first is the collinear state defined by $S_i^z = \frac{1}{2}$, for i even and $S_i^z = -\frac{1}{2}$ for i odd (this has a degeneracy 2) with an energy per site

of $E = S^2(J_{\parallel}^z - J_{\perp}^z)$. The other state is the antiferromagnetic one defined by $\pm S_i^z = \frac{1}{2}(-1)^{i/2}$ for i even and $\pm S_i^z = \frac{1}{2}(-1)^{(i+1)/2}$, for i odd (this has a degeneracy 2×2), with an energy per site of $E = -S^2 J_{\parallel}^z$. We have an Ising antiferromagnet for $J_{\perp}^z < 2J_{\parallel}^z$ and a collinear Ising ferromagnet for $J_{\perp}^z > 2J_{\parallel}^z$, with a first order transition separating the two phases.

Consider now the stiffness tensor in the classical limit. Imposing a spiral spin configuration on the zig-zag ladder with a pitch angle θ , the energy per site of the classical $J_1 - J_2$ model is then given as above by

$$e = \frac{E}{N} = S^2 J_1 \cos(\theta + \theta_1) + S^2 J_2 \cos(2\theta + \theta_2), \quad (2)$$

where we have added small twists θ_1 and θ_2 to the nearest-neighbor and the next-nearest-neighbor terms, respectively. For $\theta_1 = 0 = \theta_2$, we have that $\cos \theta_0 = -1$ for $J_1 > 4J_2$ and that $\cos \theta_0 = -\frac{1}{4}(J_1/J_2)$ for $J_1 < 4J_2$, as stated above. The spin currents are then given by

$$\begin{aligned} j_1 &= \left. \frac{\partial e}{\partial \theta_1} \right|_0 = -S^2 J_1 \sin \theta_0 \\ j_2 &= \left. \frac{\partial e}{\partial \theta_2} \right|_0 = -S^2 J_2 \sin 2\theta_0 \end{aligned} \quad (3)$$

and the rigidity components by

$$\begin{aligned} \rho_{11} &= \left. \frac{\partial j_1}{\partial \theta_1} \right|_0 = -S^2 J_1 \cos \theta_0 \\ \rho_{12} &= \left. \frac{\partial j_1}{\partial \theta_2} \right|_0 = 0 \\ \rho_{22} &= \left. \frac{\partial j_2}{\partial \theta_2} \right|_0 = -S^2 J_2 \cos 2\theta_0. \end{aligned} \quad (4)$$

Note that both the spin currents and the stiffnesses are independent of the anisotropy parameter Δ in the classical limit: the isotropic and the XY anisotropic cases give the same results. In the collinear phase at $J_1 > 4J_2$, the spin currents vanish ($j_1 = 0 = j_2$) and $\rho_{11} = S^2 J_1$, $\rho_{12} = 0$ and $\rho_{22} = -S^2 J_2$. On the other hand, in the spiral phase at $J_1 < 4J_2$ the local spin currents are non-vanishing: $j_1 = \pm S^2 J_1 [1 - (J_1/4J_2)^2]^{1/2}$ and $j_2 = -\frac{1}{2}j_1$. However, the total spin current $j_s = j_1 + 2j_2$ is null. The stiffness tensor of this spiral phase is given by $\rho_{11} = \frac{1}{4}S^2(J_1^2/J_2)$, $\rho_{12} = 0$ and $\rho_{22} = S^2[J_2 - \frac{1}{8}(J_1^2/J_2)]$. The natural stiffness associated with the total spin j_s is the response to an external twist that satisfies $\theta_2 = 2\theta_1$, and is given by $\rho_s = \rho_{11} + 4\rho_{12} + 4\rho_{22}$. It reduces to $\rho_s = S^2(J_1 - 4J_2)$ in the collinear phase and to $\rho_s = S^2[4J_2 - \frac{1}{4}(J_1^2/J_2)]$ in the spiral phase. These results are displayed in Fig. 2. Here it is shown that ρ_s is always positive and that vanishes at the classical transition point between the collinear ferromagnet to the spiral phase. Recall that the nature of the groundstate changes across this transition. Also, we remark that in the spiral phase only the stiffness ρ_s and the total current j_s

are ‘‘well behaved’’. The other components show spontaneous spin currents, while ρ_{22} is not always positive (we will return to this point later while discussing the quantum case).

In the general quantum case we calculate the stiffness in the standard way.²² We consider the Hamiltonian (1) with periodic boundary conditions imposing uniform twists around the z axis:

$$\begin{aligned} H(\theta_1, \theta_2) &= \frac{1}{2} J_1^{XY} \sum_i (S_i^+ S_{i+1}^- e^{i\theta_1} + S_i^- S_{i+1}^+ e^{-i\theta_1}) \\ &+ \frac{1}{2} J_2^{XY} \sum_i (S_i^+ S_{i+2}^- e^{i\theta_2} + S_i^- S_{i+2}^+ e^{-i\theta_2}) \\ &+ J_i^z \sum_i S_i^z S_{i+1}^z + J_2^z \sum_i S_i^z S_{i+2}^z. \end{aligned} \quad (5)$$

Here θ_1 and θ_2 are two independent twists that act separately along the interchain and intrachain directions, respectively. Expanding the exponentials to second order we obtain the form

$$\begin{aligned} H(\theta_1, \theta_2) &= H(0, 0) + \theta_1 \sum_i J_i^1 + \theta_2 \sum_i J_i^2 \\ &- \frac{1}{2} \theta_1^2 \sum_i T_i^1 - \frac{1}{2} \theta_2^2 \sum_i T_i^2 \end{aligned} \quad (6)$$

where

$$\begin{aligned} J_i^1 &= \frac{i}{2} J_1^{XY} (S_i^+ S_{i+1}^- - S_i^- S_{i+1}^+) \\ J_i^2 &= \frac{i}{2} J_2^{XY} (S_i^+ S_{i+2}^- - S_i^- S_{i+2}^+) \end{aligned} \quad (7)$$

are the spin currents along the interchain and intrachain directions, respectively and where

$$\begin{aligned} T_i^1 &= \frac{1}{2} J_1^{XY} (S_i^+ S_{i+1}^- + S_i^- S_{i+1}^+) \\ T_i^2 &= \frac{1}{2} J_2^{XY} (S_i^+ S_{i+2}^- + S_i^- S_{i+2}^+) \end{aligned} \quad (8)$$

are the kinetic energy operators. Using second-order perturbation theory, we then obtain that the groundstate stiffness tensor, $\rho_{\alpha\beta} = (\partial^2 E / \partial \theta_\alpha \partial \theta_\beta)|_0$, is given by

$$\begin{aligned} \rho_{\alpha\beta} &= - \sum_i \langle 0 | T_i^\alpha | 0 \rangle \delta_{\alpha,\beta} \\ &- 2 \sum_{\nu \neq 0} \frac{1}{E_\nu - E_0} \sum_{i,j} \langle 0 | j_i^\alpha | \nu \rangle \langle \nu | j_j^\beta | 0 \rangle, \end{aligned} \quad (9)$$

where $|0\rangle$ is the groundstate and $|\nu\rangle$ are the excited states ($\alpha, \beta = 1, 2$). The groundstate is assumed to be non-degenerate. Both the spin current operator $J^\alpha = \sum_i J_i^\alpha$ and the kinetic operator $T^\alpha = \sum_i T_i^\alpha$ commute with the translation operator, T , and conserve total spin S_z (where $\alpha = 1, 2$). Therefore, the states $|\nu\rangle$ in the stiffness formula (9) are the excited states within the

subspace of a given magnetization and momentum that contains the groundstate.

As in the classical case discussed earlier, the stiffness can also be calculated directly³⁰ taking numerical derivatives of the energy with respect to small twists, θ_1 and θ_2 , that are imposed on the system. This procedure requires care that θ_1 and θ_2 are small enough so that there be no level crossings. (We prefer to use the correlation function method, even though the results using both methods agree very well.) The change in energy due to small twists θ_1 and θ_2 takes the form

$$\delta E = \frac{1}{2}\rho_{11}\theta_1^2 + \rho_{12}\theta_1\theta_2 + \frac{1}{2}\rho_{22}\theta_2^2 \quad (10)$$

in the absence of spontaneous spin currents. It is then natural to consider the eigenvalues of the stiffness tensor

$$\rho_{\pm} = \frac{1}{2}(\rho_{11} + \rho_{22}) \pm \sqrt{\left(\frac{\rho_{11} - \rho_{22}}{2}\right)^2 + \rho_{12}^2} \quad (11)$$

and the determinant $D = \rho_+ \rho_- = \rho_{11}\rho_{22} - \rho_{12}^2$. These eigenvalues will be computed using expression (9) for the stiffness tensor in the next section.

We shall also calculate the correlation function associated with the dimerization via linear response theory. Imposing a small explicit dimerization, we consider the Hamiltonian

$$\begin{aligned} H(\delta_1, \delta_2) = & \frac{1}{2}J_1^{XY} \sum_i (1 + (-i)^i \delta_1) (S_i^+ S_{i+1}^- + S_i^- S_{i+1}^+) \\ & + \frac{1}{2}J_2^{XY} \sum_i (1 + (-i)^i \delta_2) (S_i^+ S_{i+2}^- + S_i^- S_{i+2}^+) \\ & + J_1^z \sum_i (1 + (-i)^i \delta_1) S_i^z S_{i+1}^z \\ & + J_2^z \sum_i (1 + (-i)^i \delta_2) S_i^z S_{i+2}^z. \end{aligned} \quad (12)$$

Once again using second order perturbation theory we obtain that the susceptibility $\chi_{\alpha\beta} = -(\partial^2 E / \partial \delta_\alpha \partial \delta_\beta)|_0$ is given by

$$\begin{aligned} \chi_{\alpha\beta} = & 2 \operatorname{Re} \sum_{\nu \neq 0} \frac{1}{E_\nu - E_0} \sum_{i,j} (-1)^{i+j} \\ & \langle 0 | (T_i^\alpha + M_i^\alpha) | \nu \rangle \langle \nu | (T_j^\beta + M_j^\beta) | 0 \rangle \end{aligned} \quad (13)$$

where

$$\begin{aligned} M_i^1 &= J_1^z S_i^z S_{i+1}^z \\ M_i^2 &= J_2^z S_i^z S_{i+2}^z. \end{aligned} \quad (14)$$

In the dimer correlation function, the factor $(-1)^{i+j}$ implies that the states $|\nu\rangle$ are contained in the same magnetization subspace, but in the $k = k_0 \pm \pi$ momentum subspace, where k_0 is the groundstate momentum. Last, the structure factor is defined in the usual way:

$$S(q) = \sum_r e^{iqr} C_r \quad (15)$$

where the correlation function C_r is defined by

$$C_r = \frac{1}{NS(S+1)} \sum_i \langle 0 | \vec{S}_i \cdot \vec{S}_{i+r} | 0 \rangle. \quad (16)$$

and is normalized such that the local correlation function ($r = 0$) is unity.

III. RESULTS

We now proceed to study the XXZ zig-zag model (1) using exact diagonalization of finite systems with sizes up to $N = 28$. The full energy spectrum is obtained for the smaller system sizes, $N \leq 16$, while only the groundstate and the first few excited states can be determined for the larger system sizes. The eigenvectors and eigenvalues of Hamiltonian eq. (1) are then substituted into Eqs. (9,13,15) to compute the various correlation functions. Our main aim is to study the transitions between the various phases.

Spectrum. Let us first survey the energy spectrum that is displayed by these small systems. We shall keep track of important quantum numbers associated with each energy level, such as the momentum along the rib of the zig-zag, the spin and the parity. We shall also identify points in parameter space where low-lying levels cross, and use this to identify phase transitions in the system. This procedure is known to yield accurate transition points when applied to even relatively small systems.^{9,23}

Let us begin by determining the quantum numbers of the groundstate as a function of the size N for the $S = 1/2$ zig-zag antiferromagnet. Periodic boundary conditions are imposed throughout. The groundstate is a spin singlet in general due to the antiferromagnetic interactions. For strong enough coupling between chains, $j = J_2/J_1 < 1/2$, it has either momentum π for $N = 4n+2$ or momentum 0 for $N = 4n$. For weak enough coupling between chains $j > 1/2$, on the other hand, the momentum oscillates between 0 and π as a function of the coupling parameter j and of the system size N .²⁴ There are several points along j in this regime where the corresponding energy levels for these two momentum values cross. The groundstate is degenerate at these points, and this is reflected by peaks in the dimer correlation function (see Fig. 8). Such level crossings grow in number as the system size grows, and this indicates that the two singlet states in question are in fact degenerate in the thermodynamic limit. By the Lieb-Schultz-Mattis theorem,²⁵ this is consistent with a spin gap in the excitation spectrum that survives the thermodynamic limit in the weak-coupling regime $j > 1/2$.

Consider now the specific case of an XXZ zig-zag chain (1) with $N = 16$ sites under periodic boundary

conditions (see Table I). In the isotropic case, $\Delta = 1$, the states are organized into spin triplets due to the $SU(2)$ spin invariance. Again, the antiferromagnetic interactions imply that the groundstate is a spin singlet ($S_z = 0$) in general. The system has three well defined regimes: (a) strong-coupling, (b) intermediate coupling and (c) weak-coupling. In the strong-coupling limit (a), $j = J_2/J_1 \rightarrow 0$, the groundstate has momentum $k = 0$. The first excited state forms a spin triplet in such case, with $k = \pi$, while the second excited state is another spin singlet with $S_z = 0$ and $k = \pi$. At $j = j_{c1}^N \sim 0.24$ there is a level crossing where the first excited states and the second excited state interchange (here j_{c1}^N is the value of j at which the level crossing occurs for the system with size N). In the thermodynamic limit the two lowest singlet states ($S_z = 0, k = 0$ and $S_z = 0, k = \pi$) become degenerate and there is a finite gap to the next excited state (the triplet state $S_z = 0, \pm 1, k = \pi$). Although the system begins to dimerize at this stage (b), antiferromagnetic correlations along the rib of the zig-zag remain dominant up to the Majumdar-Ghosh point²⁶ at $j = 1/2$. The groundstate is doubly degenerate for any system size at this point, where the two states are perfectly dimerized. Antiferromagnetic correlations *within* chains of the zig-zag become dominant beyond this point at weaker couplings $j > 1/2$ (see Fig. 9). Another level crossing occurs as j increases to about $j_{c2}^N \sim 1.6$ such that the first excited states become two triplets with $S_z = 0, \pm 1, k = \pm\pi/2$. The groundstate displays quantum numbers $S_z = 0$ and $k = 0$ at this stage (c), and it is no longer degenerate. This remains so as $j \rightarrow \infty$. It should be mentioned, however, that White and Affleck predict that a non-zero spin gap persists in the thermodynamic limit at weak-coupling $j \gg 1$ between chains, and that it becomes exponentially small as j grows¹³ (we will return to this point later).

The spectrum of the anisotropic $S = 1/2$ XXZ zig-zag ladder has also been studied previously in the strong-coupling regime up to the Majumdar-Ghosh line ($0 < j < 1/2$).²⁷ A gapless regime occurs for XY anisotropy $\Delta \leq 1$ and strong coupling $j < j_{c1}(\Delta)$, an Ising antiferromagnet along the rib of the zig-zag that shows a spin gap in the excitation spectrum occurs for $\Delta > 1$ and $j < j_{c1}(\Delta)$, and a dimer phase regime that also has a spin gap exists at $j > j_{c1}(\Delta)$ and any Δ (here $j_{c1}(\Delta)$ is the transition line obtained from extrapolation to the thermodynamic limit). The line $j = j_{c1}(\Delta)$ separates the gapless phase from the dimer phase for $\Delta \leq 1$, while it separates the dimer phase from the (Ising) Néel phase for $\Delta > 1$. The line at $\Delta = 1$ and $j < j_{c1}$ separates the XY gapless phase from the Ising phase.

Consider again the specific case of $N = 16$ sites in this instance, with anisotropy parameters $\Delta = 0$ or $\Delta = 0.5$ (see Table I). The groundstate is a singlet with $S_z = 0$ and $k = 0$ as j increases from the strong coupling limit at $j = 0$ up to $j = 1/2$. The first excited state has degeneracy 2, with spin $S_z = \pm 1$ and momentum $k = \pi$ inside this regime. The next excited state is again a sin-

glet with $S_z = 0$ and $k = \pi$. As j increases there exists a line of points, $j = j_{c1}^N(\Delta)$, such that the energy level of the excited state with $S_z = \pm 1, k = \pi$ crosses the energy level of the excited state $S_z = 0, k = \pi$.²⁷ For $j > j_{c1}^N(\Delta)$ the two lowest states are the two singlets with $S_z = 0, k = 0$ and $S_z = 0, k = \pi$. Again, these two states become degenerate (with a gap to the first excited state) in the thermodynamic limit. The groundstate must be a spin singlet with $S_z = 0$ due to the antiferromagnetic couplings. This excludes the possibility that any $S_z = \pm 1$ state be degenerate with it. As a result, the level crossing between the $S_z = \pm 1$ and singlet states can be used as an accurate criterion to determine the phase transition between the gapless and the spin-gap regimes.⁹ If we increase j up to $j = 1/2$, then the system is exactly degenerate for all system sizes. This is a feature of the Majumdar-Ghosh point, which has a perfectly dimerized groundstate. The behavior of the system does not change much for intermediate coupling $j > 1/2$ beyond this point, with the exception that the momentum of the two lowest states interchanges between $k = 0$ and $k = \pi$ as j grows. At a larger value of $j = j_{c2}^N$ between 1.2 – 1.6, however, a level crossing occurs between the $S_z = 0, k = 0$ or π state (first excited state) and a state with $S_z = \pm 1, k = \pi/2$ (second excited state). Notice that the momentum of the first excited state is now $k = \pi/2$. This is to be expected in this regime since the two chains are weakly coupled, and the periodicity doubles. For $j > 2$, in particular, the first excited state is now four-fold degenerate ($S_z = \pm 1, k = \pm\pi/2$), and we might expect to fall back into a gapless regime since the first excited state is not a spin singlet. This level structure is in fact the same as for $j \rightarrow \infty$.

In Fig. 3 we present the crossing points between the states $S_z = 0, k = \pi$ and $S_z = \pm 1, k = \pm\pi/2$ that signal this transition as function of the number of sites for several values of the anisotropy parameter Δ . We have attempted to extrapolate the crossing points, j_{c2}^N , to the thermodynamic limit by employing a standard (BST) algorithm due to Bulirsch and Stoer.²⁸ The method is explained in the Appendix. The results of this extrapolation procedure are shown in Fig. 4, where j_{c2} is plotted as a function of Δ . The curve j_{c2} separates a spin-gap (dimer) phase from a gapless phase at small interchain couplings. As expected the value of j_{c2} grows near the isotropic point. (It should tend to $j = \infty$ at $\Delta = 1$ according to White and Affleck.¹³)

Physical Probes. Correlation functions can also be used to determine the nature of different thermodynamic groundstates. The spin rigidity, in particular, can discriminate between phases that do and do not have spin gaps. The stiffness of the nearest-neighbor spin-1/2 Heisenberg chain has been calculated exactly via the Bethe ansatz.²² In the thermodynamic limit this solution yields

$$\frac{\rho_{11}}{J_1^{XY}} = \frac{\pi}{4} \sin \frac{\pi}{n} \frac{1}{\left(\pi - \frac{\pi}{n}\right)} \quad (17)$$

for anisotropies

$$\cos \frac{\pi}{n} = \frac{J_1^z}{J_1^{XY}} = \Delta, \quad (18)$$

where n is a positive integer. This yields $\rho_{11}/J_1^{XY} = 1/4$ in the isotropic case and $\rho_{11}/J_1^{XY} = 1/\pi$ in the XY -case. In Fig. 5 we plot the exact Bethe ansatz stiffness²² for the single chain and compare it with the numerical diagonalization results for $N = 8, 12, 16, 20$ sites. The spectrum is gapless from the XY -limit up to the isotropic Heisenberg case. Beyond this critical point the spectrum acquires a gap due to the Ising anisotropy and the stiffness goes to zero. The stiffness remains positive beyond the transition point for the small system sizes that we studied, however. The anisotropy at which $\rho_{11} = J_1^{XY}/4$ extrapolates nicely to the Heisenberg point, $\Delta = 1$, in the thermodynamic limit, $N \rightarrow \infty$, however.

The zigzag ladder (or the chain with next-nearest neighbor interactions), on the other hand, is not solvable by the Bethe ansatz, and so other methods become necessary to compute the spin rigidity. With this purpose in mind, exact diagonalization calculations of the isotropic spin-1/2 Heisenberg chain with next-nearest neighbors interactions were carried out first by Bonca et al.³⁰ on small systems, where the diagonal component ρ_{11} of the stiffness tensor was computed (see also ref. 31). We have completed this study by calculating the remaining components of the stiffness tensor (9), including cases with anisotropy. In Fig. 6 we show the results for the various stiffnesses for the zigzag ladder in the isotropic case as a function of j for $N = 16$, while the same set of results are shown for the XY -case ($\Delta = 0$) in Fig. 7. In Figs. 6a and 7a we show the stiffnesses ρ_{11} , ρ_{22} and ρ_{12} . For small j we are in the limit of strong interchain coupling (small next-nearest neighbor interaction) and we recover the previous results:³⁰ $\rho_{11} > 0$ and $\rho_{22} < 0$. This is also found in the classical case. In the opposite weak-coupling limit of very high j , ρ_{11} remains negative, but ρ_{22} becomes positive (as in the classical case). The latter is consistent with the extreme limit of two decoupled antiferromagnetic chains ($J_1 = 0$). Also, ρ_{12} becomes non-zero in the intermediate region where quantum fluctuations are stronger and where the transition between weak-coupling and strong-coupling occurs. Note that the classical analysis reveals that the fact that ρ_{12} becomes nonzero and the fact that ρ_{11} becomes negative are purely quantum effects.

In the initial exact diagonalization study for the isotropic case, Bonca et al. chose to identify the point at which the stiffness component ρ_{11} turns negative with a transition point to a quantum disordered phase with a spin gap.³⁰ Extrapolating to the thermodynamic limit they estimated the transition point to occur at $j_c = 0.270 \pm 0.005$. We believe that it is a better idea to look at the eigenvalues (11) of the full stiffness tensor to determine possible phase transitions.³² In Figs. 6b and 7b we plot ρ_+ for different system sizes. This stiffness is always positive for all j , while ρ_- is always negative. For

small j , ρ_+ is positive and of order unity. As j grows ρ_+ becomes close to zero at a value of j that is close to the value where ρ_{11} crosses zero, $j_{\rho_1}^N$. As j increases further ρ_+ again begins to grow appreciable near the point at which ρ_{22} turns positive, $j_{\rho_2}^N$. A finite size analysis reveals that as the size N grows the first “zero” of ρ_+ (near $j = j_{\rho_1}^N$) occurs at smaller values of j and extrapolates to a value close to the dimer transition j_{c1} determined by the level-crossing method. Similarly, we expect that the second transition to a nonzero stiffness ρ_+ (near $j = j_{\rho_2}^N$) signals the transition to a gapless regime that extends up to $j = \infty$, and that it might therefore also signal a decoupling transition. This happens, however, both for $\Delta = 0$ and for $\Delta = 1$. We believe that this is due to a finite-size effect in the latter case as discussed above. The fact that finite-size effects in the spin stiffness of a single chain become larger as the XY anisotropy decreases (see Fig. 5) supports this claim.

The level crossing at weak-coupling, j_{c2}^N , does not, however, correlate well with $j_{\rho_2}^N$. The crossings defined by $j_{\rho_2}^N$ appear at smaller values of j as compared with j_{c2}^N . Although both have the same trend, apparently finite size effects are stronger in the calculation of the stiffness than in the determination of the level crossings. We have therefore limited ourselves to the extrapolation of the level crossing points j_{c2}^N .

In Fig. 8 we show the behavior of the dimer correlation function χ_{11} . For $j > j_{c1}^N$ the dimer correlation function increases signaling the spontaneous dimerization observed in the thermodynamic limit. The various peaks signal level crossings of the groundstate between near-degenerate states with momentum $k = 0$ and $k = \pi$ as j varies. The Majumdar-Ghosh point at $j = 1/2$ is special since the groundstate is doubly degenerate for all system sizes in such case. Beyond $j \sim 1$ the dimer correlation function χ_{11} becomes small. (The susceptibilities χ_{12} and χ_{22} are always quite small).

Finally, remnants of the spiral phase that exists in the classical limit, $S \rightarrow \infty$, are clearly apparent in the momentum dependence of the structure factor. In Fig. 9 we show the structure factor as a function of momentum for several values of j in the Heisenberg case at $\Delta = 1$. We see that the location of the maximum shifts from $k_{max} = \pi$ (for $j \leq 0.5$) to a value $\pi/2 < k_{max} < \pi$ when $j > 0.5$, thereby signaling the spiral phase. The results are similar for $\Delta = 0$.

IV. CONCLUSIONS

The $S = 1/2$ antiferromagnetic zig-zag ladder is a difficult problem to solve due to the intrinsic frustration and to the criticality displayed by both the strong and the weak-coupling limits. The weak-coupling limit is particularly difficult in the absence of anisotropy, in

which case antiferromagnetic correlations diverge exponentially.¹³ This renders any numerical study of finite systems hard.

In this paper, we have performed an analysis of the exact properties of such finite systems, looking at various correlation functions and the structure of the spectrum both in the isotropic and the anisotropic cases. We have looked at the spectrum and have computed the spin stiffness of the zig-zag ladder, and have thereby found evidence for a gapless regime at weak coupling that survives the thermodynamic limit in the case of XY anisotropy. However, the isotropic and the anisotropic cases look qualitatively similar. We believe that this is due to a strong finite-size effect in the former case. This claim is supported by the increase of finite-size effects in the stiffness of a single $S = 1/2$ antiferromagnetic chain with decreasing XY anisotropy, as shown in Fig. 5.

It was previously shown⁹ that the dimer transition can be accurately determined in relatively small systems by studying the level crossing of the first and second excited states after extrapolating to the thermodynamic limit. We have used a similar criterion to detect a possible transition from the dimer phase to a gapless phase at weak-inter chain coupling. Using standard extrapolation techniques (see Appendix) we have constructed a phase diagram (see Fig. 4) in this regime that is in agreement with a recent proposal for a gapless spiral phase in the presence of XY anisotropy.¹⁵

Also, we expect the spin stiffness ρ_+ to be a good measure of the nature of the spectrum. In particular, it can be used as an order parameter to distinguish gapless from spin-gap phases. A positive stiffness indicates a gapless excitation spectrum and a null stiffness indicates a net spin-gap. The antiferromagnetic zig-zag for spin $S = 1/2$ showed an appreciable positive stiffness in the limit of strong interchain coupling (similar to the single chain case), a very small yet positive stiffness in the intermediate (spin-gap) regime, and then again an appreciable positive stiffness in the limit of weak interchain coupling (similar to two decoupled chains). This was true for all values of the (XY) anisotropy, $\Delta \leq 1$. It is known from previous work,¹³ however, that a spin gap is always expected to be present in the isotropic case at weak coupling. The stiffness should therefore remain zero in the thermodynamic limit at $\Delta = 1$ in the weak-coupling regime. We believe that the discrepancy between this expectation and our results is a strong finite size effect in the isotropic case that is due to the exponentially diverging antiferromagnetic correlations.¹³ Clearly, larger systems need to be studied.

Acknowledgments

We have benefited from helpful discussions and comments from Didier Poilblanc, Alexander Nersesyan, Fabian Essler and Alexander Gogolin. We are also indebted to Ed Rezayi for suggesting the spectral analysis.

APPENDIX:

Exact Diagonalization. The size of the Hilbert space under consideration can be considerably reduced using the symmetries of the problem. The Hamiltonian commutes with the total spin operator S_T^z , with the translation operator T , the spin flip operator R , and the space reflection operator L ($i \rightarrow N+1-i, i = 1, \dots, N$). In the absence of anisotropies the Hamiltonian also commutes with the total spin operator $(\vec{S}_T)^2$ and the energy levels come in spin multiplets.

The operator R commutes with T but, although L commutes with R , it does not commute with T , since $LT = T^{-1}L$.

The action of the local operators S_i^\pm and S_i^z is simply given in the direct product basis $|m_1^z \rangle \dots |m_N^z \rangle$, which are eigenvectors of S_T^z . In general, these states are not eigenvectors of the additional symmetries. We consider first the translations, obtaining the classes of states which are closed under them. One starts with a state $|a \rangle$ and applies N_a times the translation operator T until one finds $T^{N_a}|a \rangle = |a \rangle$, where N_a is necessarily a divisor of N . The state $|a \rangle$ is the representative of this class. In combinatorial theory this is called a necklace and its periodic part, of length N_a , a Lyndon word. The other classes are formed proceeding in the same manner starting with other states, not already used, until all the states have been exhausted. In each class, since $T^{N_a} = \hat{1}$, the possible eigenvectors of T are $t_{N_a}(k) = e^{\frac{i2\pi k}{N_a}}$, with $k = 0, \dots, N_a - 1$, corresponding to the momentum $p_k = \frac{2\pi k}{N_a}$. The operators $P_N(k) = \frac{1}{N} \sum_{i=0}^{i=N-1} (\frac{T}{t_N(k)})^i$ are projectors, i.e, they satisfy $P_N(k)P_N(k') = \delta_{k,k'}P_N(k)$. They also have the property $TP_N(k) = t_N(k)P_N(k)$. The projector $P_N(k)$ acting on the states of a class with N_a elements reduces to $\frac{N}{N_a}P_{N_a}(k)$, if $t_N(k)$ is one of the $t_{N_a}(k)$ and gives zero otherwise. The normalized eigenvector of momentum p_k formed from the class of the state $|a \rangle$ is given by $|k, a \rangle = \sqrt{N_a}P_{N_a}(k)|a \rangle$. Since the Hamiltonian commutes with S_T^z and T , the subspaces of fixed magnetization and momentum are invariant subspaces and it is important to consider each of these subspaces separately. A general state is written as a linear combination of the states $|k, a \rangle$ corresponding to that magnetization. The state $|k, a \rangle$ is represented by $|a \rangle$. This allows us to reduce the size of the basis to the number of representatives.

The spin reflection changes the sign of the magnetization. Therefore it is relevant only for the classification of the states when the magnetization is zero. If $R|a \rangle$ is not in the class of $|a \rangle$ both eigenvectors with $r = 1$ and $r = -1$ can be formed. If $R|a \rangle$ is in the class of $|a \rangle$, it must be obtained from this state by $\frac{N_a}{2}$ translations (implying that N_a must be even), since for half-integer spin it is linearly independent of $|a \rangle$. The state $|k, a \rangle$ is an eigenvalue of R with $r = 1$ for k even and $r = -1$

for k odd.

The space reflection operator reverses the momentum, since one has $LP_N(k) = P_N(-k)L$. The state $L|a\rangle$ can be in a different class or in the same class. The states $|k, a\rangle$ and $|-k, a\rangle$ are linearly independent, except for $k = 0$, with eigenvalue $l = 1$, or $k = \frac{N_a}{2}$, for N_a even, with eigenvalue $l = -1$. As a result, one sees that, for zero magnetization and $t = \pm 1$, it is possible to use all the operators T, R and L in the construction of the states. This allows a further reduction of the size of the subspace under consideration. Since some classes have a definite eigenvalue of R or L they are simply excluded if their values are not those of the state which we are studying.

Since the complete Hamiltonian commutes with the operator T only transitions to states with the same momentum are allowed, even if separate terms in the Hamiltonian allow them. If $H|a\rangle = \sum_b \alpha T^{p(a,b)}|b\rangle$, where $p(a,b)$ is an integer and $|b\rangle$ is the representative of a class, one finally finds $\langle k, b|H|k, a\rangle = \sum_b' \alpha \sqrt{\frac{N_a}{N_b}} (t_{N_a}(k))^{p(a,b)}$, where the summation is restricted to the allowed transitions.

The modified Lanczos method¹⁹ is very useful to obtain the ground state of an Hamiltonian. Restricting our attention to a subspace of fixed magnetization and momentum we will find the ground state of the block Hamiltonian in that subspace. To obtain an approximate ground state we choose a trial state $|\psi_0\rangle$ that can not be orthogonal to the true ground-state. We define a state $|\psi_1\rangle$ as¹⁹

$$|\psi_1\rangle = \frac{\hat{H}|\psi_0\rangle - \langle H \rangle |\psi_0\rangle}{(\langle H^2 \rangle - \langle H \rangle^2)^{1/2}} \quad (\text{A1})$$

where $\langle \psi_1|\psi_1 \rangle = 1$, $\langle \psi_1|\psi_0 \rangle = 0$ and $\langle H^n \rangle = \langle \psi_0|\hat{H}^n|\psi_0 \rangle$. Defining a matrix of the Hamiltonian in the basis $|\psi_0\rangle, |\psi_1\rangle$ we can diagonalize it¹⁹ obtaining a next order approximation for the energy $\tilde{\epsilon}_0$, and ground state $|\tilde{\psi}_0\rangle$, with

$$\tilde{\epsilon}_0 = \langle H \rangle + b\alpha \quad (\text{A2})$$

$$|\tilde{\psi}_0\rangle = \frac{|\psi_0\rangle + \alpha|\psi_1\rangle}{(1 + \alpha^2)^{1/2}} \quad (\text{A3})$$

where

$$b = (\langle H^2 \rangle - \langle H \rangle^2)^{1/2} \quad (\text{A4})$$

$$\alpha = f - (f^2 + 1)^{1/2} \quad (\text{A5})$$

and

$$f = \frac{\langle H^3 \rangle - 3\langle H \rangle\langle H^2 \rangle + 2\langle H \rangle^3}{2(\langle H^2 \rangle - \langle H \rangle^2)^{3/2}}. \quad (\text{A6})$$

Taking $|\tilde{\psi}_0\rangle$ as the new $|\psi_0\rangle$ we can iterate the method to obtain a better estimate for the energy and the ground state.

Since the ground state and the first excited of the system have different momenta they are both ground states of different subspaces, and we apply the modified Lanczos method to these subspaces. If the system does not have anisotropies one can alternatively look for the component of the spin multiplet of the first excited state with magnetization 1.

Extrapolation. The results for the infinite system can be estimated using standard extrapolation methods like the BST method.²⁸ In the BST algorithm we look for the limit of a sequence of the type $T(h_j) = T + a_1 h_j^\omega + a_2 h_j^{2\omega} + \dots$, $j = 0, \dots, N_p - 1$ (N_p being the number of data points), where h_j is a sequence converging to zero as $j \rightarrow \infty$, corresponding to different system sizes N_j . Typically $h_j = \frac{1}{N_j}$, with $N_j = a + bj$, for some values of a, b . The value of the m^{th} iteration for the sequence is obtained from

$$T_m^{(j_m)} = T_{m-1}^{(j_m+1)} + \frac{T_{m-1}^{(j_m+1)} - T_{m-1}^{(j_m)}}{\left(\frac{h_{j_m}}{h_{j_m+m}}\right)^\omega \left(1 - \frac{T_{m-1}^{(j_m+1)} - T_{m-1}^{(j_m)}}{T_{m-1}^{(j_m+1)} - T_{m-2}^{(j_m+1)}}\right)} - 1 \quad (\text{A7})$$

with $j_m = 0, \dots, M(m)$ and where $M(m)$ is the number of values of $T_m^{(j_m)}$ at each iteration. It decreases by one, at each iteration, from $M(0) = N_p$ to $M(N_p - 1) = 1$, when the iteration process is fulfilled. As initial values one defines $T_{-1}^{(j)} = 0$ and $T_0^{(j)} = T(h_j)$. The extrapolated value is $T_{N_p-1}^{(0)}$ and the estimated error is $\epsilon = |T_{N_p-2}^{(1)} - T_{N_p-2}^{(0)}|$. Finally, ω is a free parameter which is adjusted such that the estimate of the error is a minimum.

¹ E. Dagotto and T.M. Rice, Science **271**, 618 (1996).

² F.D.M. Haldane, Phys. Rev. Lett. **45**, 1358 (1980).

³ S. Chakravarty, B.I. Halperin and D.R. Nelson, Phys. Rev. Lett. **60**, 1057 (1988).

⁴ T. M. Rice, Z. Phys. B **103**, 165 (1997).

⁵ F.D.M. Haldane, Phys. Rev. Lett. **50**, 1153 (1983).

⁶ T. Barnes, E. Dagotto, J. Riera and E.S. Swanson, Phys. Rev. B **47**, 3196 (1993).

⁷ J.P. Rodriguez, P.D. Sacramento and V.R. Vieira, Phys. Rev. B **56**, 13685 (1997).

⁸ R. Coldea et al., J. Phys. Cond. Matt. **8**, 7473 (1996); Phys. Rev. Lett. **79**, 151 (1997).

⁹ K. Okamoto and K. Nomura, Phys. Lett. A **169**, 433 (1992).

¹⁰ S. Eggert, Phys. Rev. B **54**, R9612 (1996).

¹¹ P. Wind, N. Guihéry, J.P. Malrieu, Phys. Rev. B **59**, 25 (1999).

¹² R. Chitra, S. Pati, H.R. Krishnamurthy, D. Sen and S. Ramasesha, Phys. Rev. B **52**, 6581 (1995).

¹³ S.R. White and I. Affleck, Phys. Rev. B **54**, 9862 (1996).

- ¹⁴ D. Allen and D. Sénéchal, Phys. Rev. B **55**, 299 (1997).
- ¹⁵ A.A. Nersesyan, A.O. Gogolin and F.H.L. Essler, Phys. Rev. Lett. **81**, 910 (1998).
- ¹⁶ M. Kaburagi, H. Kawamura and T. Hikihara, J. Phys. Soc. Jpn. **68**, 3185 (1999).
- ¹⁷ A. A. Aligia, C. D. Batista and F. H. L. Essler, cond-mat/0002318.
- ¹⁸ T. Hikihara, M. Kaburagi and H. Kawamura, cond-mat/0007095.
- ¹⁹ E.R. Gagliano, E. Dagotto, A. Moreo and F.C. Alcaraz, Phys. Rev. B **34**, 1677 (1986).
- ²⁰ E.R. Davidson, J. Comp. Phys. A **17**, 87 (1975).
- ²¹ R.J. Baxter, Ann. Phys. (N.Y.) **70**, 193 (1972).
- ²² B.S. Shastri and B. Sutherland, Phys. Rev. Lett. **65**, 243 (1990).
- ²³ T. Tonegawa, I. Harada and M. Kaburagi, J. Phys. Soc. Jpn. **61**, 4665 (1992).
- ²⁴ T. Tonegawa and I. Harada, J. Phys. Soc. Jpn. **56**, 2153 (1987).
- ²⁵ E.H. Lieb, T. Schultz and D.J. Mattis, Ann. Phys. NY **16**, 407 (1961); I. Affleck and E.H. Lieb, Lett. Math. Phys. **12**, 57 (1986).
- ²⁶ C.K. Majumdar and D.K. Ghosh, J. Math. Phys. **10**, 1388 (1969).
- ²⁷ K. Nomura and K. Okamoto, J. Phys. Soc. Jpn. Lett. **62**, 1123 (1993); J. Phys. A: Math. Gen. **27**, 5773 (1994).
- ²⁸ See for example, M. Henkel and G. Schutz, J. Phys. A: Math. Gen. **21**, 2617 (1988); P. D. Sacramento and V. R. Vieira, J. Phys. Cond. Matter. **9**, 10687 (1997).
- ²⁹ An alternative way to determine a transition into a spin-gap phase is to extrapolate the values of the gaps for spin excitations in the two regimes to the thermodynamic limit. This is a difficult numerical problem because it is hard to distinguish between a very small gap and a null gap.
- ³⁰ J. Bonca, J.P. Rodriguez, J. Ferrer and K.S. Bedell, Phys. Rev. B **50**, 3415 (1994).
- ³¹ T. Einarsson and H.J. Schulz, Phys. Rev. B **51**, 6151 (1995).
- ³² The stiffness can be negative for finite systems even though it is expected to be either zero or positive for infinite systems. In the thermodynamic limit, a negative stiffness means that the system is unstable. In the case of a finite system it may mean that the true groundstate is incommensurate with the system size considered (see ref. 31).

Table I- Lowest energy levels for $N = 16$. The states are represented by their S_z values and momenta $(S_z; k)$. When more than one state is represented this means they are degenerate. When the momenta are not 0, π or $\pi/2$ the momentum of the state is represented by an integer, n , such that $k = \frac{2\pi}{N}n$.

j	$\Delta = 0$	$\Delta = 0.5$	$\Delta = 1$
	(2; π)	(0; 0)	(0, 1, 2; 0, π)
	(0; π)	(0; π)	(0; $\pi/2$)
	(1; $\pi/2$)	(1; $\pi/2$)	(0, 1; $\pi/2$)
10	(0; 0)	(0; 0)	(0; 0)
	(2; π)	(0; 0)	(0; $\pi/2$)
	(0; π)	(0; π)	(0; π)
	(1; $\pi/2$)	(1; $\pi/2$)	(0, 1; $\pi/2$)
2	(0; 0)	(0; 0)	(0; 0)
	(2; π)	(0; $\pi/2$)	(0; $\pi/2$)
	(0; π)	(1; $\pi/2$)	(0, 1; $\pi/2$)
	(1; $\pi/2$)	(0; π)	(0; π)
1.5	(0; 0)	(0; 0)	(0; 0)
	(0; π)	(0; π)	
	(1; $\pi/2$)	(1; $\pi/2$)	(0, 1; $\pi/2$)
	(0; π)	(0; π)	(0; π)
1	(0; 0)	(0; 0)	(0; 0)
	(1; 3)	(1; 3)	(0, 1; π)
	(0; π)	(0; π)	(0, 1; 3)
	(0; 0)	(0; 0)	(0; 0)
0.75	(0; π)	(0; π)	(0; π)
	(0; 0)	(1; 1)	(0, 1; 1)
	(1; π)	(1; π)	(0; 0)
	(0; π)	(0; π)	(0, 1; π)
0.5	(0; 0, π)	(0; 0, π)	(0; 0, π)
	(0; π)	(0; π)	(0, 1; 1)
	(0; π)	(0; π)	(0, 1; π)
	(1; π)	(1; π)	(0; π)
0.25	(0; 0)	(0; 0)	(0; 0)
	(0; π)	(0; π)	(0, 1; 1)
	(0; π)	(0; π)	(0; π)
	(1; π)	(1; π)	(0, 1; π)
0.1	(0; 0)	(0; 0)	(0; 0)

Figure Captions

Fig. 1- Diagram of the zig-zag ladder. The nearest-neighbor interaction is parameterized by J_1 and the next-nearest-neighbor interaction is parameterized by J_2 .

Fig. 2- Classical stiffnesses $\rho_{11}/(J_1 S^2)$, $\rho_{22}/(J_1 S^2)$ and $\rho_s/(J_1 S^2)$ as a function of $j = J_2/J_1$.

Fig. 3- Crossing points of the first excited state as a function of N for different values of Δ at weak coupling.

Fig. 4- Phase diagram in the regime of weak interchain coupling. The critical coupling parameter j_{c2} is obtained from the crossing of the first excited state with the second excited state after extrapolating to the thermodynamic limit (see the Appendix).

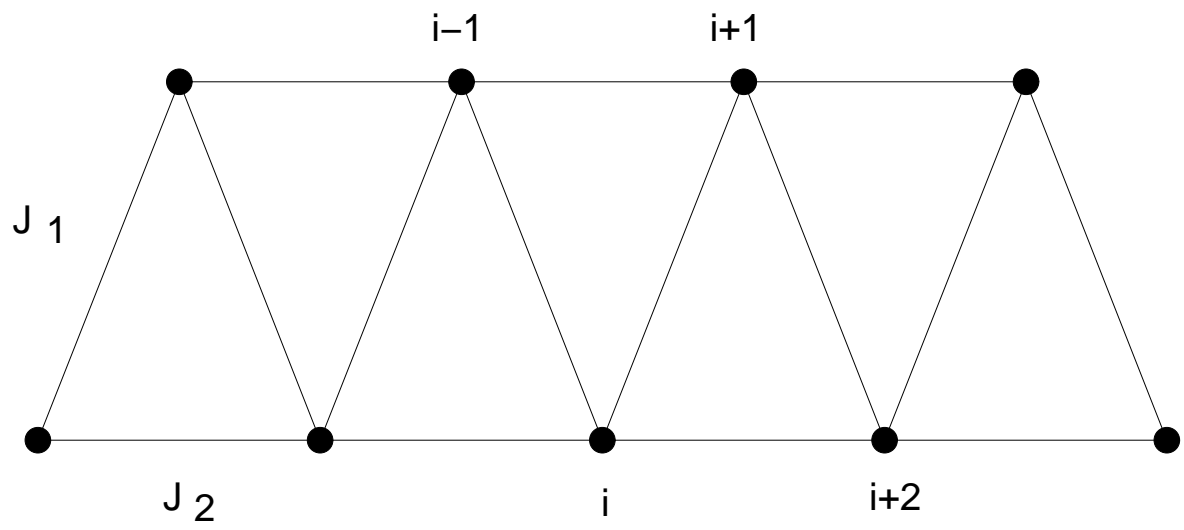
Fig. 5- Comparison of the exact Bethe ansatz result for the spin stiffness of a single chain to the numerical results obtained from diagonalizing small systems as a function of Δ .

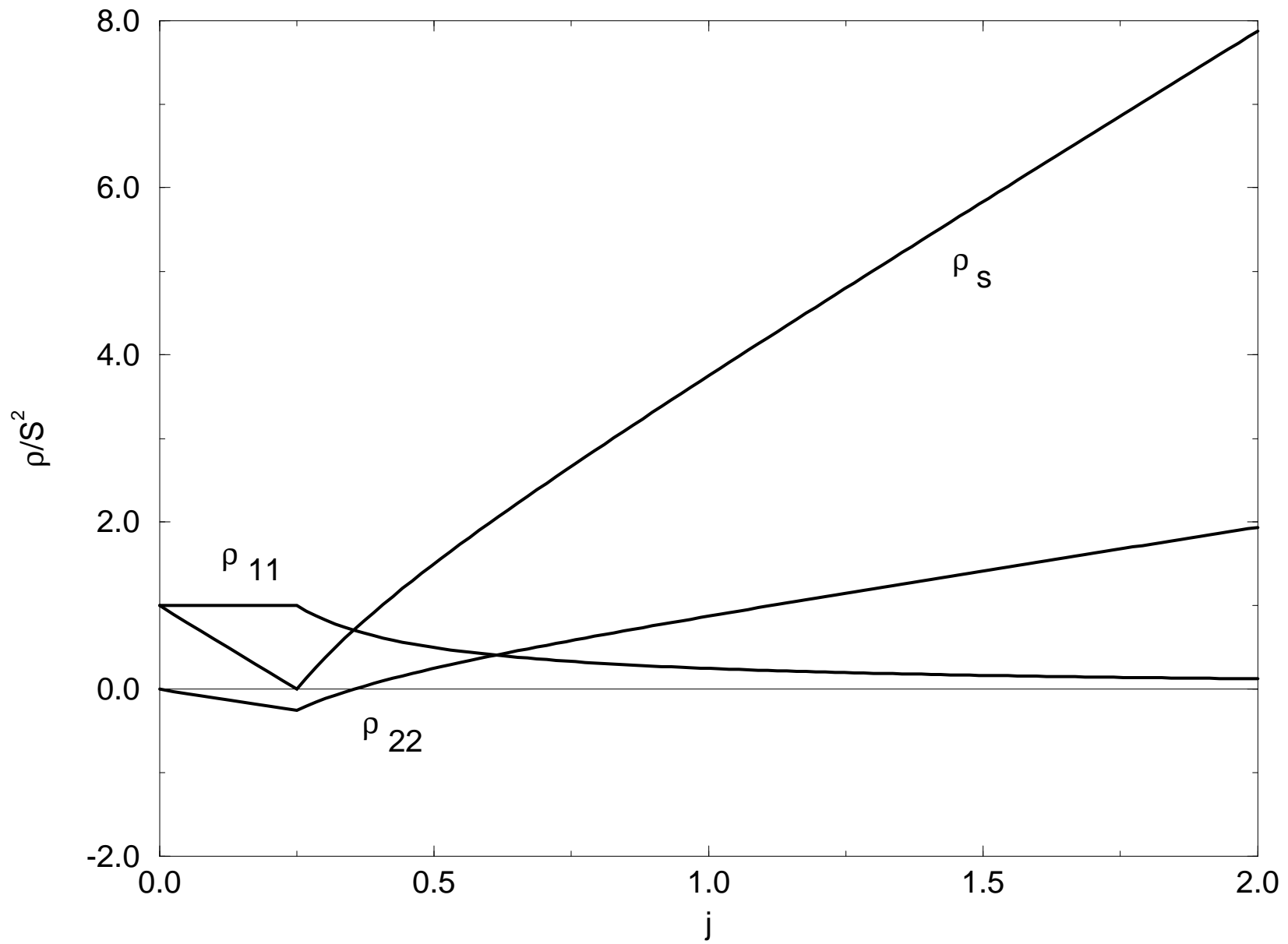
Fig. 6- (a) Stiffnesses ρ_{11} , ρ_{12} and ρ_{22} as a function of j for $\Delta = 1$ and $N = 16$. (b) ρ_+ as a function of j for various system sizes for $\Delta = 1$.

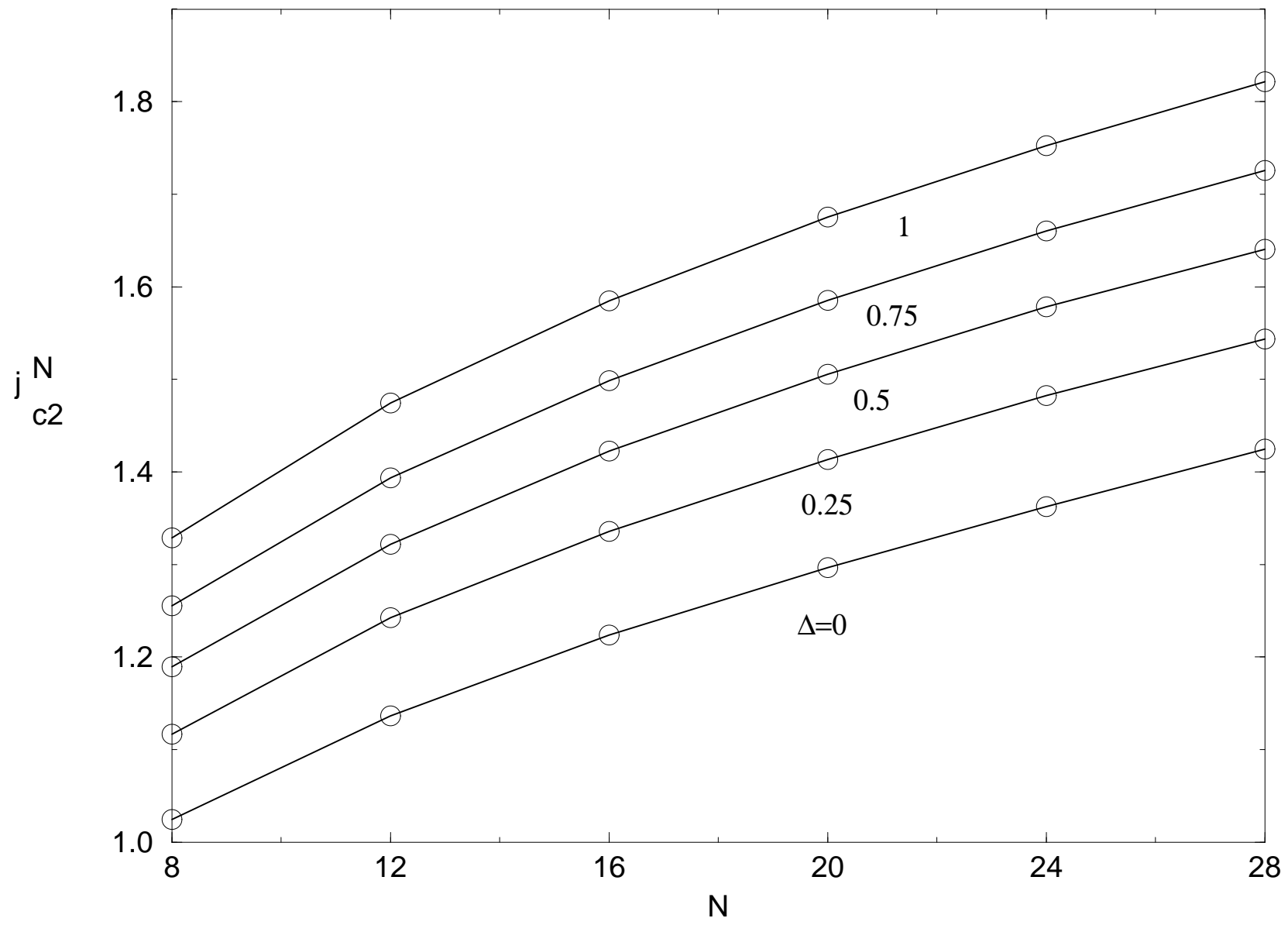
Fig. 7- (a) Stiffnesses ρ_{11} , ρ_{12} and ρ_{22} as a function of j for $\Delta = 0$ and $N = 16$. (b) ρ_+ as a function of j for various system sizes for $\Delta = 0$.

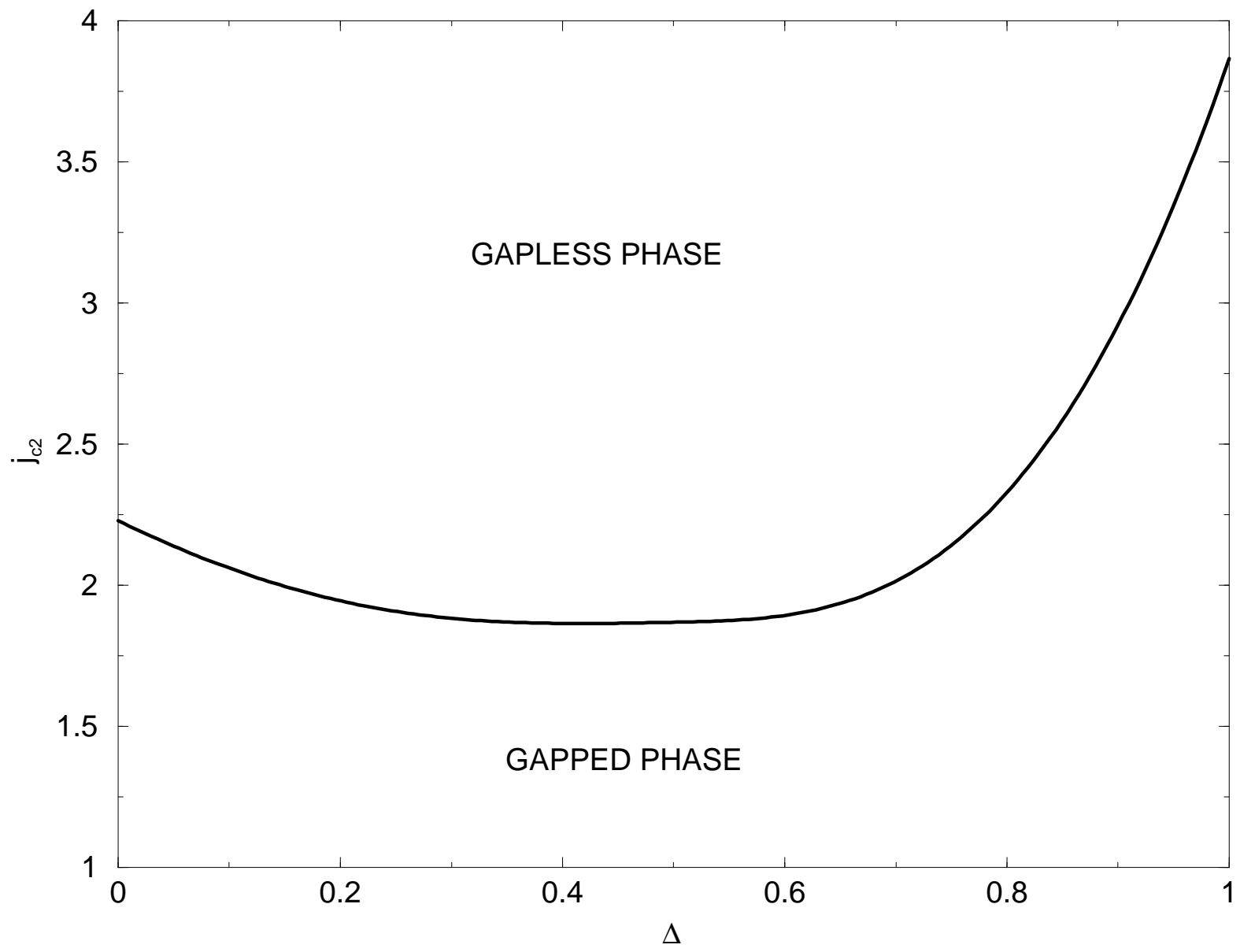
Fig. 8- Dimer correlation function for $N = 16$ and $\Delta = 1$ and $\Delta = 0$.

Fig. 9- Structure factor, $S(q)$, for $N = 16$ and $\Delta = 1$ for various coupling strengths. The peak is located at $q = \pi$ in the single-chain limit, $j = 0$ but this momentum tends to $q = \pi/2$ as j increases. This indicates the presence of important spiral correlations in the weakly-coupled $S = 1/2$ zig-zag antiferromagnet.









S=1/2 Antiferromagnetic Chain

